Reply to Comments

The manuscript presents the development of a new global marine gravity model, NSOAS24, which utilizes updated data from multiple nadir satellite altimetry missions, including HY-2. The manuscripts address limitations in a previous model, NSOAS22, also developed by the lead author. The authors proposed several technical improvements, including boundary inconsistencies, dataset filtering, near-shore area processing, and re-designing step sizes. The NSOAS24 model has comparable performance compared to the Sandwell & Smith model and DTU model. The work is relevant and aligns well with the ongoing need for high-resolution marine gravity models for applications in geophysics, oceanography, and remote sensing. My primary concern is that the authors compare NSOAS24 against the Sandwell & Smith V32.1 and DTU21 models, which use a shorter timespan of nadir satellite radar altimetry data. Including an explanation of this discrepancy in the manuscript would enhance clarity. Overall, I see no major technical issues and recommend a minor revision.

Dear reviewer:

The author's team would like to thank you very much for taking your valuable time to review the paper and for providing very valuable feedback and suggestions.

NSOAS24, V32.1 and DTU21 have slight difference in the input multi-satellite altimeter dataset. For instance, the combination of HY-2 data is unique for NSOAS24, while the other two models also used extra sentinel-3 data. Therefore, we did not analyze the specific differences in involved missions and data lengths between these models.

We have carefully read your review comments and respond to each of your feedback below. The black font is your review comments, the red font is the explanatory response, and the blue font is the revision in the revised manuscript.

Detailed comments:

1. Need to introduce DTU21, SS V32.1 in the abstract.

   Thanks for the suggestion. We have added the introduction of DTU21 and SS V32.1 in the abstract of the revised manuscript. The new abstract is shown below in blue text.

   Abstract

   Judging from the early release of the NSOAS22 model, there were some known issues, such as boundary connection problems in block-wise solutions and a relatively high noise level. By solving these problems, a new global marine gravity model NSOAS24 is derived based on sea surface slopes (SSS) from multi-satellite altimetry missions. Firstly, SSS and along-track deflections of vertical (DOV) are obtained by retracking, resampling, screening, differentiating, and filtering procedures on basis of altimeter waveforms and sea surface height measurements. Secondly, DOVs with a 1'x1' grid interval are further determined by the Green's function method, which applies directional gradients to constrain the surface, least-square fit to constrain noisy points, and tension constraints to smooth the field. Finally, the marine gravity anomaly is recovered from the gridded DOV according to the Laplace Equation. Among the entire processing procedures, accuracy improvements are expected for NSOAS24 model due to the following changes, e.g., supplementing recent mission observations and removing ancient mission data, optimizing the step size during the Green's function method, and special handling in near-shore areas. These optimizations effectively resolved the known issues of signal aliasing and the “hollow phenomenon” in coastal zones. The typical altimetry-derived marine gravity models are the DTU series released by the Technical University of Denmark and the S&S series released by the Scripps Institution of Oceanography (SIO), University of California San Diego (UCSD). Their latest models, DTU21 and SS V32.1, were used for comparison and validation. Numerical verification was conducted in three experimental areas (Mariana Trench area, Mid-Atlantic Ridge area, Antarctic

area, representing low, mid and high latitude zones) with DTU21, SS V32.1 and shipborne data. Taking NSOAS22 for contrast, NSOAS24 showed improvements of 1.2, 0.7, 1.0 mGal in 3 test areas by validating with SS V32.1, while declines of 0.6, 0.5, 0.3 mGal, and 0.2, 0.4, 0.3 mGal occurred in STD statistics with DTU21 and shipborne data. Finally, the NSOAS24 was assessed using two sets of shipborne data (the early NCEI dataset and the lately dataset from JAMSTEC, MGDS, FOCD, and SHOM) on global scale. Generally, NSOAS24(6.33 and 4.95 mGal) showed comparable accuracy level with DTU21 (6.20 and 4.71 mGal) and SS V32.1 (6.40 and 5.53 mGal), and better accuracy than NSOAS22 (6.64 mGal and 5.64 mGal). Besides, the new model is available at https://doi.org/10.5281/zenodo.12730119.

2. In Figure 1e, what are the stripes? Given CryoSat-2's inclination of 92°, one would expect N-S aligned stripes rather than the NW-SE pattern depicted.

   The stripes are caused by the satellite's trajectory. Yes, CryoSat-2's inclination is 92°, as shown in the figure below. This is the data distribution of a CryoSat-2 pass near the equator. It can be observed that the data distribution does not form perfectly N-S aligned stripe, but rather follows the NW-SE pattern depicted. Therefore, in Figure 1(e), such stripes are consistent with the trajectory distribution of the CryoSat-2 satellite.

Figure 1. A distribution map of CryoSat-2 data for a pass near the equator

3. Figure 2 caption: in dashed rectangular ◊ in dashed rectangle.

   Thank you for your reminder. All corrections have been made in the revised manuscript.

4. Equation 1: Ensure that every parameter in Equation 1, including 'N,' is defined within the text to avoid ambiguity.

   Thanks for the suggestion. All changes have been made in the revised manuscript according to your suggestions. The modifications in the revised manuscript are shown below in blue text.

$$\varepsilon^{\alpha} = -\frac{\partial N}{\partial s} = -\frac{\partial N}{\partial t} * \frac{\partial t}{\partial s} = -\frac{\partial N}{\partial t} * \frac{1}{v} \qquad (1)$$

   Here, N is the height of the geoid, s is the spherical distance, and t is the observation time. The process for determining the linear velocity v is as follows. Given a data point's latitude φ, we first convert the geodetic latitude to geocentric latitude φ_c by considering the Earth's flattening e. The formula is expressed as follows:

5. Line 276: what are the wavelengths used in the Parks-McClellan filter? Need to provide the wavelength range used for this study.

   In marine gravity anomaly inversion, models derived from nadir altimeters achieve an accuracy of approximately 2–3 mGal and require low-pass filtering at wavelengths of at least 14 km to suppress short-wavelength noise amplified by differential derivative calculations (Sandwell et al., 2021). Therefore, we referenced this standard and applied a Parks-McClellan filter with a cutoff diameter of 16 km. We have included a description of this section in the revised manuscript.

   Reference

   Sandwell, D.T., Harper, H., Tozer, B., Smith, W.H.F.: Gravity field recovery from geodetic altimeter missions. Adv. Space Res., 68, 1059–1072, https://doi.org/10.1016/j.asr.2019.09.011, 2021.

6. Line 281: what is sea surface topography? Is it mean dynamic topography? If so authors should to use this standardized term.

   Thank you for your reminder. It is mean dynamic topography. All corrections have been made in the revised manuscript.

7. Figure 8 is very hard to read. Authors could possibly consider using histogram to compare the noise level and noise points alternatively.

   Thanks for the suggestion. The histogram has been added according to your suggestion.

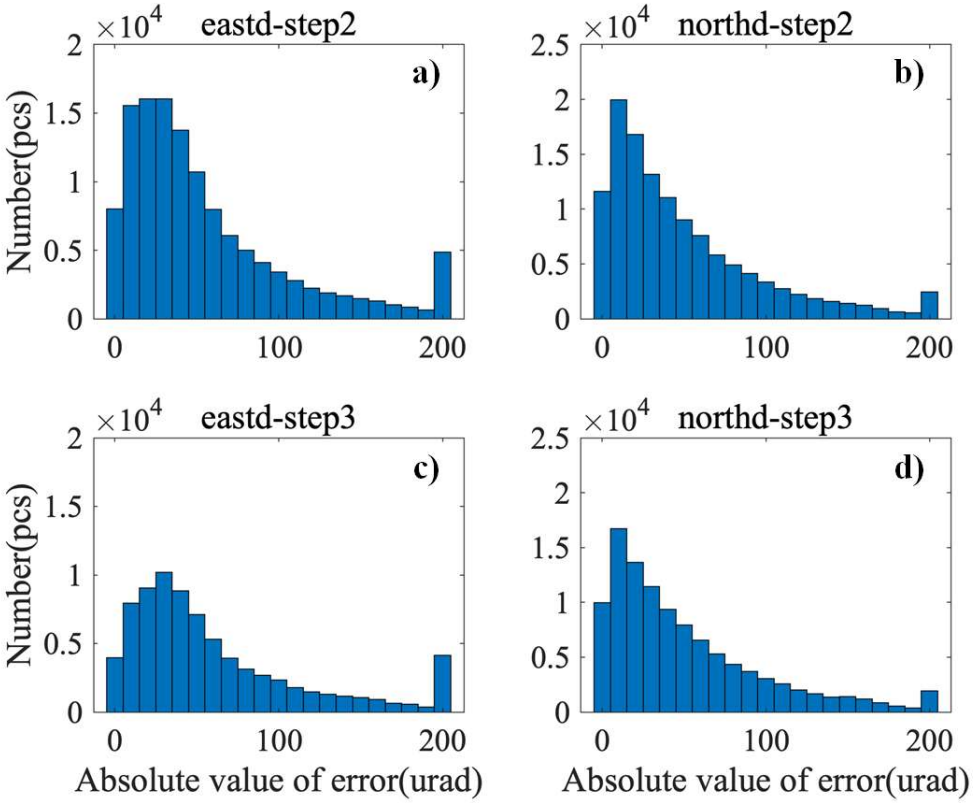

Figure 1. Noise histogram with different step sizes (a: east-west component at step size 2; b: north-south component at step size 2; c: east-west component at step size 3; d: north-south component at step size 3)

8. Color bars (figures 7,8,10,11,14): The current colorbar make it challenging to distinguish between red and dark pink. Could consider color-blind-friendly colormaps such as turbo, or blue to red when showing differences in Figures 10 and 11.

   Thanks for the suggestion. Based on your suggestions, we have re-plotted the figures using blue-to-red colormaps. The new figures are shown below.

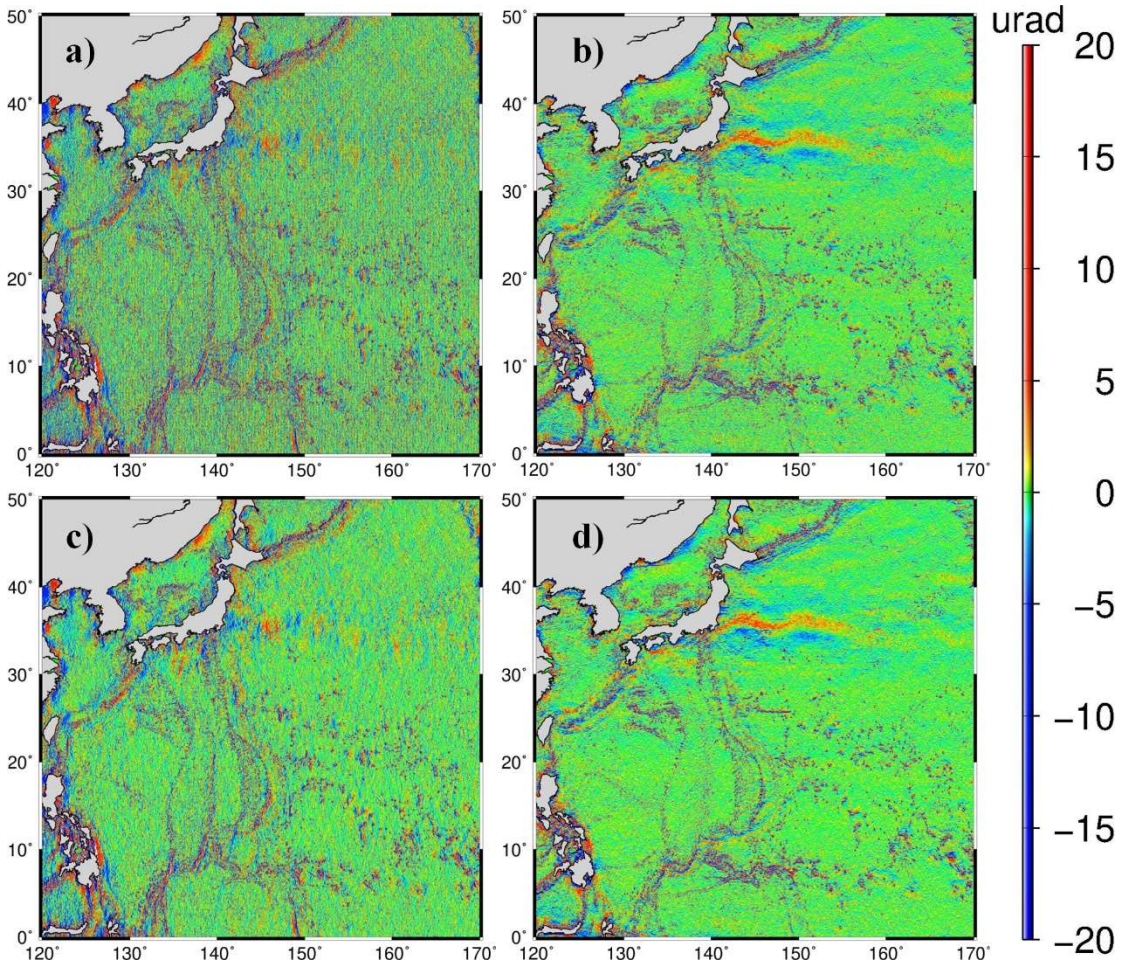

Figure 7. Residual results of DOV components difference for different step size selections (a: east-west component at 2 steps; b: north-south component at 2 steps; c: east-west component at 3 steps; d: north-south component at 3 steps)

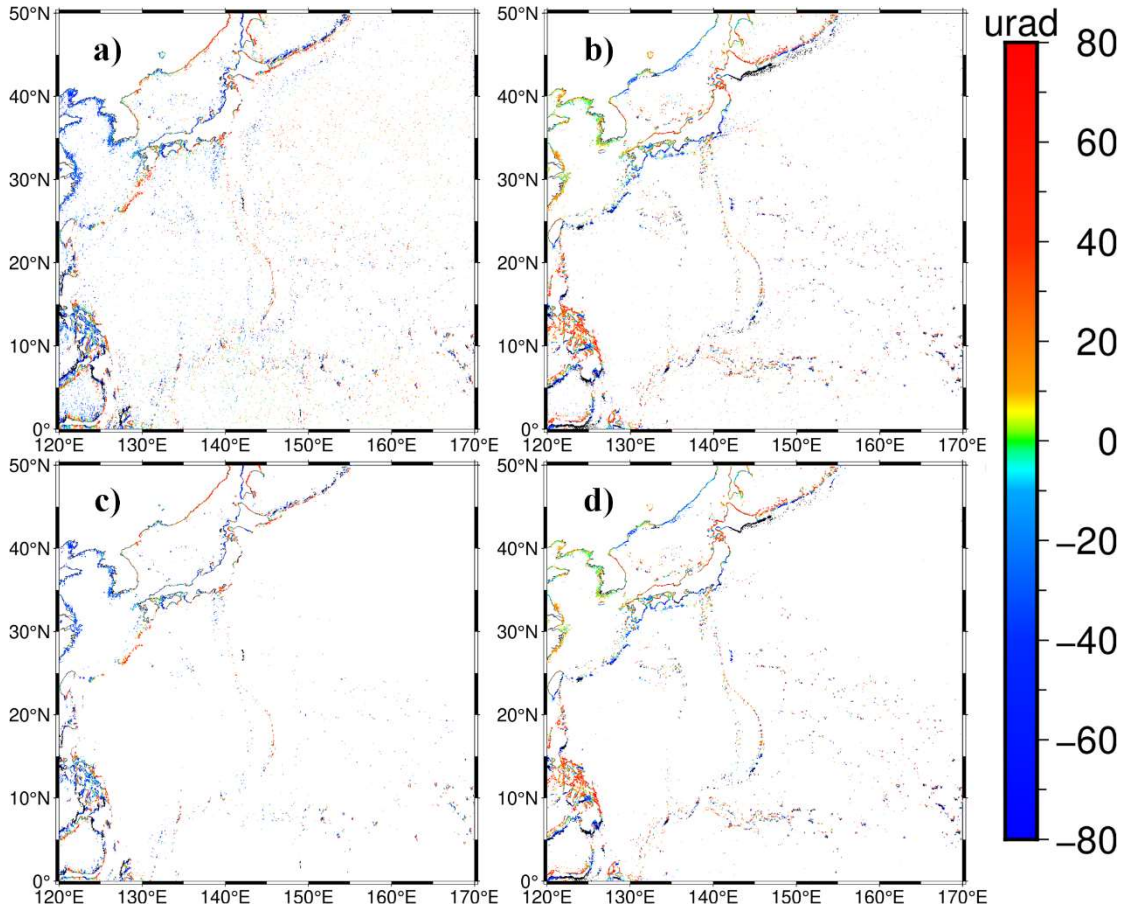

Figure 8. Noise analysis at different step sizes (a: east-west component at step size 2; b: north-south component at step size 2; c: east-west component at step size 3; d: north-south component at step size 3)

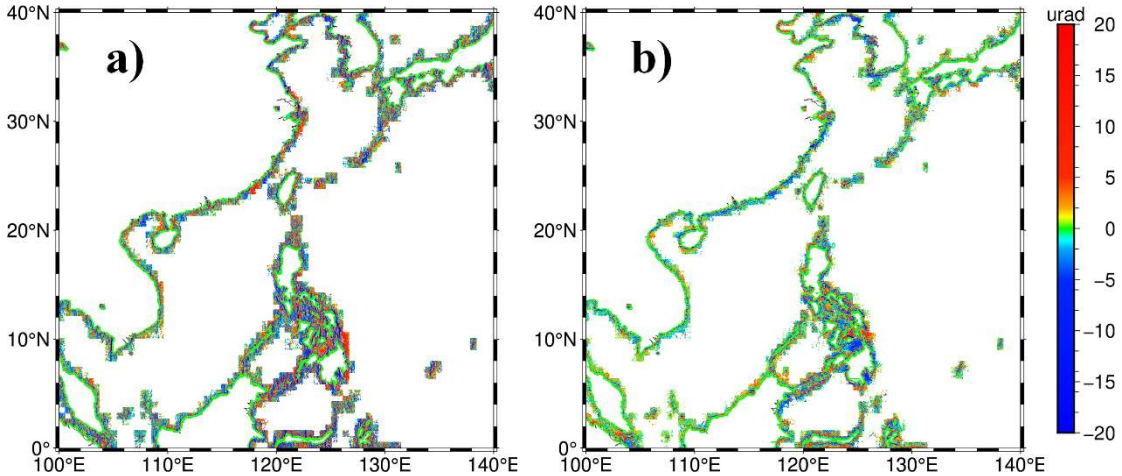

Figure 10. Location of distribution of nearshore areas disturbed by continental regions (a: east-west component; b: north-south component)

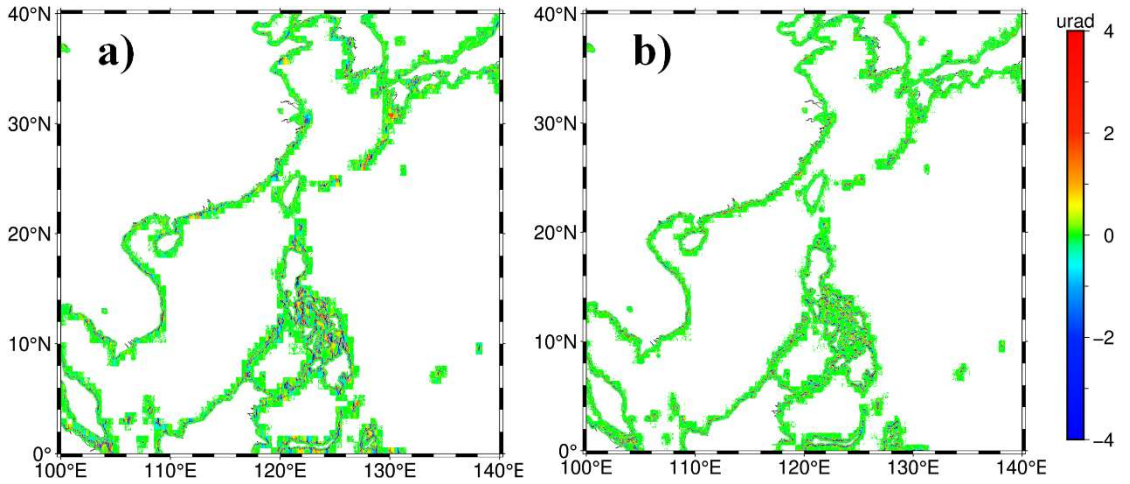

Figure 11. Difference in results in the nearshore area before and after the special processing (a: east-west component; b: north-south component)

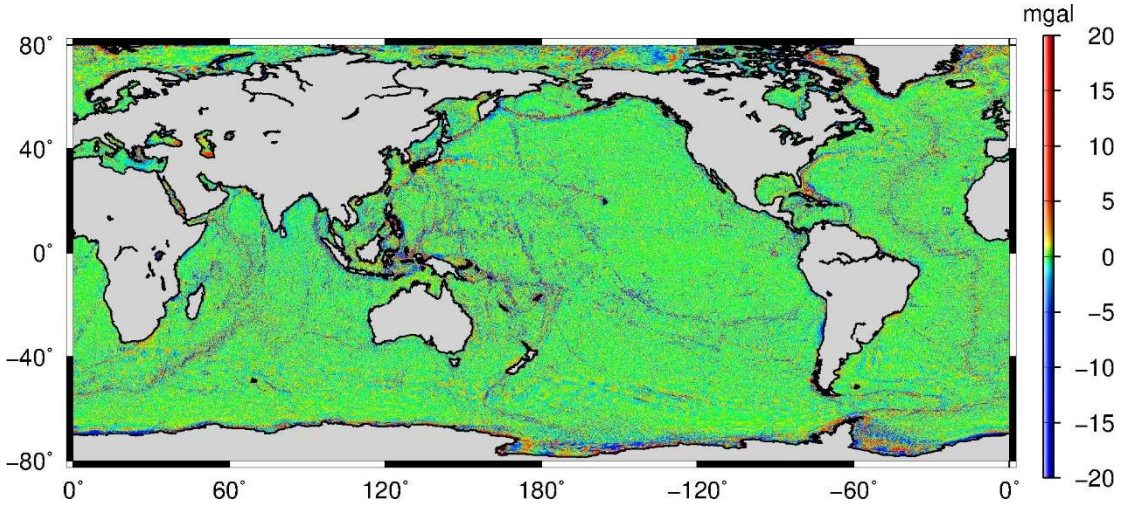

Figure 14. The residual gravity anomaly map of NSOAS24